Robust second-order correlation of twin parametric beams generated by amplified spontaneous parametric down-conversion

Kunpeng Jia (贾琨鹏)[1], Xiaohan Wang (汪小涵)[1], Xinjie Lü (吕新杰)[1], Ping Xu (徐 平)[1,2], Zhenlin Wang (王振林)[1], Chee Wei Wong (黄智维)[3], Gang Zhao (赵 刚)[1,*], Yan-Xiao Gong (龚彦晓)[1,], Zhenda Xie (谢臻达)[1,***], and Shining Zhu (祝世宁)[1]**

[1]*National Laboratory of Solid State Microstructures, School of Physics, School of Electronic Science and Engineering, College of Engineering and Applied Sciences, and Collaborative Innovation Center of Advanced Microstructures, Nanjing University, Nanjing 210093, China*

[2]*Institute for Quantum Information and State Key Laboratory of High Performance Computing, College of Computing, National University of Defense Technology, Changsha 410073, China*

[3]*Mesoscopic Optics and Quantum Electronics Laboratory, University of California Los Angeles, California, CA 90095, USA*

**Corresponding author: zhaogang@nju.edu.cn; **corresponding author: gongyanxiao@nju.edu.cn; ***corresponding author: xiezhenda@nju.edu.cn*

Received June 12, 2020; accepted August 21, 2020; posted online October 16, 2020

We report an observation of the second-order correlation between twin beams generated by amplified spontaneous parametric down-conversion operating above threshold with kilowatt-level peak power, from a periodically poled $LiTaO_3$ crystal via a single-pass scheme. Photocurrent correlation was measured because of the bright photon streams, with raw visibility of 37.9% or 97.3% after electronic filtering. As expected in our theory, this correlation is robust and insensitive to parametric gain and detection loss, enabling important applications in optical communications, precision measurement, and nonlocal imaging.

Keywords: amplified spontaneous parametric down-conversion; robust second-order correlation; high-gain twin beams.

doi: 10.3788/COL202018.121902.

The second-order correlation of light was first detected from the light generated by classical thermal radiation on star surfaces[1]. Since then, this correlation has been a long-lasting interest and serves as the heart of modern quantum optics because it was recognized as a new "nonlocal" optical coherence effect involving optical fields at two different space–time points[2]. Later, the research was extended to investigate the characteristic of nonclassical light, especially entangled photon pairs generated by spontaneous parametric down-conversion (SPDC). The surprising correlation features, which can only be interpreted by quantum mechanics without classical equivalence[3–8], have led to many promising applications in various photonic quantum technologies[9–14].

However, this second-order correlation may not be limited to the single-photon level, as the inherent correlation of the photon pairs should still exist when the amplification occurs and the gain scales up in the parametric process. From the application point of view, there is strong motivation to investigate the correlation between twin beams in the high-gain regime because of the fragility of single photons and the relatively poor performance of the electro-optical devices working at the single-photon level. To date, however, the second-order correlation in such a gain regime has not been studied in detail[15–22]. The nonclassical features in a high-gain parametric process can only be demonstrated by the complicated quadrature measurements[23–27], which are highly sensitive to the gain level and photon loss, and thus much less robust compared to the correlation measurement.

In this Letter, we report an observation of the second-order correlation between twin beams generated by an amplified SPDC (ASPDC) process. In our experiment, the parametric down-conversion is spontaneously generated and then amplified in the same periodically poled $LiTaO_3$ (PPLT) crystal to a macroscopic power level, with high conversion efficiency under a single-pass quasi-phase-matched scheme, while the correlated features of the twin beams are well preserved. We detect 37.9% visibility from the direct correlation measurement by using well-matched narrowband filters, which is close to the 50% visibility predicted by theory. The visibility can be further enhanced to 100% with electronic filtering on the photon current. In particular, the second-order correlation between high-efficiency and high-gain twin beams above the parametric threshold is observed with traditional linear response detectors placed at two different space–time points. Moreover, this correlation is robust and does not depend on the parametric gain and detection loss. Such robust correlation of ASPDC may have important applications in broad areas of quantum information and quantum optics.

ASPDC can be viewed as a nonlinear optical analogy of the amplified spontaneous emission (ASE) process in laser gain media[28–30]. Similar to ASE, ASPDC can take place above the threshold in high-gain nonlinear media, and the conversion efficiency is much higher than SPDC. On the other hand, ASPDC differs from ASE as a second-order nonlinear optical process, where the signal and idler photons are intrinsically correlated.

Considering a plane-wave pump light illuminating a nonlinear crystal, we can write the single-mode operator of the parametric down-conversion as[31]

$$\hat{U} = \exp\left[\chi \int \mathrm{d}\omega_s \mathrm{d}\omega_i \delta(\omega_s + \omega_i - \omega_p)\hat{a}_s^\dagger(\omega_s)\hat{a}_i^\dagger(\omega_i) - \mathrm{H.c.}\right], \tag{1}$$

where χ is the gain parameter. Here, for simplicity, considering that the bandwidth of the filters at the detectors in our experiment is much narrower than the phase-matching bandwidth, we have neglected the phase-matching spectrum function. The state generated from ASPDC can be calculated by performing the operator on the vacuum state[32],

$$|\psi\rangle = \hat{U}|0\rangle = \frac{1}{\cosh|\chi|}\sum_n^\infty \frac{1}{n!}[e^{i\phi}\tanh|\chi| \times \int \mathrm{d}\omega_s \mathrm{d}\omega_i \delta(\omega_s + \omega_i - \omega_p)\hat{a}_s^\dagger(\omega_s)\hat{a}_i^\dagger(\omega_i)]^n|0\rangle, \tag{2}$$

where $e^{i\phi} = \chi/|\chi|$. In the spontaneous case, $|\chi| \ll 1$, only the first-order expansion dominates, and Eq. (2) presents an SPDC two-photon state. On the other hand, when $|\chi| \gg 1$, all of the expansions need to be considered, so the terms with large n dominate. In this case, the output state of Eq. (2) becomes a complicated multi-photon state, with all the possible superpositions of the two n-photon states. Despite its complexity, the ASPDC state still reserves similar features as the SPDC state, with an even total photon number. Moreover, the δ function ensures the frequency correlation between each pair of signal and idler photons when they are generated from the same pump photon. Because of the high parametric gain, each frequency mode may have a high photon occupation number. Similar to the case of SPDC, this frequency correlation can be characterized by the second-order correlation measurement at different space–time points $(\vec{r}_1, t_1)$ and $(\vec{r}_2, t_2)$, respectively.

The second-order correlation function is given by

$$G_{1,2}^{(2)}(t_1, t_2) = \langle\psi|\hat{E}_1^\dagger(t_1)\hat{E}_2^\dagger(t_2)\hat{E}_2(t_2)\hat{E}_1(t_1)|\psi\rangle, \tag{3}$$

where $\hat{E}_k(t)$ $(k = 1, 2)$ represent the electric field operators at the two detectors D_1 and D_2 in the signal and idler modes, respectively, expressed as

$$\hat{E}_k(t) = \frac{1}{\sqrt{2\pi}}\int \mathrm{d}\omega f_k(\omega)\hat{a}_k(\omega)e^{-i\omega t}, \tag{4}$$

with $f_k(\omega)$ denoting the transmission spectrum functions of the filters. In our experiment, the normalized transmission spectrum function can be described as $f_1(\omega) = (\Delta\omega/\pi)^{1/2}/[\Delta\omega + i(\omega - \Omega_s)]$ and $f_2(\omega) = (\Delta\omega/\pi)^{1/2}/[\Delta\omega + i(\omega - \Omega_i)]$, where $\Delta\omega$ is the filter bandwidth, and Ω_s, Ω_i are the central frequencies satisfying $\Omega_s + \Omega_i = \omega_p$.

In the practical case, however, the coherence time of the ASPDC beam is on the order of picoseconds, which is smaller than that of the fast detectors. Therefore, the response time may play an important role in the measured correlation. The measured second-order correlation $R_{1,2}^{(2)}$ can be calculated by averaging over detection response time T_R, and, by defining $\tau = t_2 - t_1$, we obtain the measured normalized correlation function as

$$\gamma^{(2)}(\tau) = \frac{R_{1,2}^{(2)}}{R_s R_i} = \begin{cases} 1 + \frac{2e^{-\Delta\omega|\tau|}[\cosh(\Delta\omega T_R) - 1]}{\tanh^2|\chi|\Delta\omega^2 T_R^2}, & |\tau| \geq T_R, \\ 1 + \frac{2[(T_R - |\tau|)\Delta\omega + e^{-\Delta\omega T_R}\cosh(\Delta\omega\tau) - e^{-\Delta\omega|\tau|}]}{\tanh^2|\chi|\Delta\omega^2 T_R^2}, & |\tau| < T_R, \end{cases} \tag{5}$$

where R_k $(k = 1, 2)$ are the measured first-order correlation function of $G_k^{(1)} = \langle\psi|\hat{E}_k^\dagger(t_k)\hat{E}_k(t_k)|\psi\rangle$, written as

$$R_k = \frac{1}{T_R}\int_t^{t+T_R} G_k^{(1)}\mathrm{d}t = \sinh^2|\chi|. \tag{6}$$

Then, the visibility can be calculated as

$$V = \frac{\gamma^{(2)}(0) - \gamma^{(2)}(\infty)}{\gamma^{(2)}(0)} = \frac{2(T_R\Delta\omega + e^{-\Delta\omega T_R} - 1)}{\tanh^2|\chi|\Delta\omega^2 T_R^2 + 2(T_R\Delta\omega + e^{-\Delta\omega T_R} - 1)}. \tag{7}$$

For the ideal case of $T_R = 0$, we arrive at the ideal second-order correlation function,

$$\gamma^{(2)}(\tau) = 1 + \tanh^{-2}|\chi|e^{-\Delta\omega|\tau|}, \tag{8}$$

with the visibility calculated as $V \approx 1/(1 + \tanh^2|\chi|)$. Hence, in the low-gain extreme, namely, the SPDC, we have $V \approx 1$, while for the ASPDC with a high gain, the visibility decreases, and, when $|\chi| \to \infty$, we have $g^{(2)}(0) \approx 2$, with the visibility approaching 50%. The shape of the correlation is determined by the modulus square of the Fourier transformation of the filtering spectrum $f_2(\omega_i)f_1(\omega_p - \omega_i)$.

It should be noted that although the normalized second-order correlation for thermal light $\gamma_{\mathrm{thermal}}^{(2)}(0)$ also equals two, the correlation of ASPDC is totally different from that of thermal light, as it originates from a two-party twin beam. As shown in Fig. 1, the correlation of thermal light actually arises from the same frequency mode of the same thermal light source and can only be detected at two different space–time points with artificial separation using

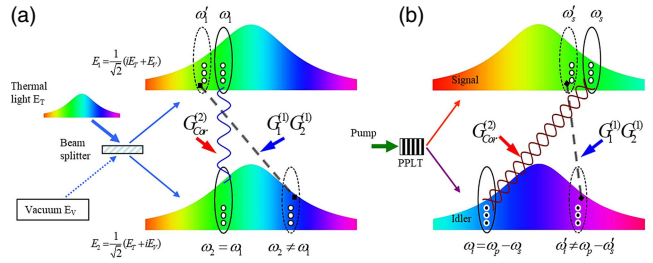

Fig. 1. Comparison of the second-order correlation of thermal light and ASPDC. (a) Thermal light correlation. The thermal light E_T is mixed with vacuum field E_V at a beam splitter. Therefore, the light fields E_1 and E_2 are from the same source even though $G^{(2)}_{1,2}$ is measured at different space–time points. $G^{(2)}_{1,2}$ can be expressed as $G^{(2)}_{1,2} = G^{(2)}_{\mathrm{Cor}} + G^{(1)}_1 G^{(1)}_2$, where the correlated term $G^{(2)}_{\mathrm{Cor}}$ comes from the same frequency components in the two split beams, and the background term $G^{(1)}_1 G^{(1)}_2$ comes from different frequency components in the two split beams. (b) ASPDC correlation. The temporal correlation can be measured directly between the signal and idler beams, where the correlated term $G^{(2)}_{\mathrm{Cor}}$ comes from signal frequency mode ω_s and its inherently correlated counterpart in idler mode $\omega_i = \omega_p - \omega_s$, while the background term $G^{(1)}_1 G^{(1)}_2$ comes from the random combination with ω'_s and $\omega'_i \neq \omega_p - \omega'_s$.

a beam splitter. For the case of ASPDC, however, the correlation feature is attributed to the inherent correlation between the signal and idler beams, because temporal correlation is a direct representation of the twin-beam correlation in the frequency domain.

For the nonideal case of $T_R \neq 0$, the visibility decreases, and, when $\Delta\omega T_R \to \infty$, the visibility approaches zero. Hence, the detector response time T_R needs to be comparable to the coherence time of the twin beam for the temporal correlation measurement. To achieve this condition, in the following experiment, we use a pair of "matched" narrowband fiber Fabry–Perot cavities (FFPCs) to filter out two portions of signal and idler beams, respectively. In Fig. 2, we plot the simulated results for the visibility

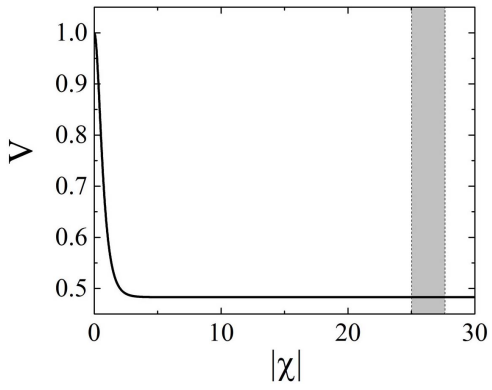

Fig. 2. Simulated visibility as a function of gain parameter. The visibility drops from one to about 48.3%, as the parametric process transforms from SPDC to ASPDC. The two vertical bars mark the range of the gain level achieved in our experiment, where the visibility can be considered as constant.

against the gain by utilizing the experiment parameters of $\Delta\omega = 2\pi \times 1.1$ GHz, $T_R = 30$ ps, which shows that the visibility approaches 48.30%, which is lower than 50% due to the nonzero T_R. For our source in the following experiment, $|\chi|$ varies from 25.2 around threshold to 27.6 at the maximum power level, as marked in Fig. 2, with almost no visibility change. As a result, the second-order correlation of the twin beams from the ASPDC process is robust to the gain change.

The schematic of our experiment setup is shown in Fig. 3. We use a 4-cm-long PPLT crystal to realize a high-gain ASPDC process. Since PPLT provides a large effective nonlinear coefficient and high damage threshold, ASPDC can be achieved above threshold without a cavity. With a poling period of 7.9 μm, the quasi-phase-matching condition of a nondegenerate parametric process can be achieved at 280°C for 532 nm(p) → 810 nm(s) + 1550 nm(i). In order to eliminate any feedback caused by Fresnel reflection, both end-facets of the PPLT crystal are anti-reflection coated for the pump, signal, and idler wavelengths, and the output face is a 1° wedged cut.

The 532 nm pump source is a single-longitudinal-mode frequency-doubled yttrium-aluminum-garnet laser (Powerlite, Continuum), with pulse duration of 5 ns and a repetition rate of 10 Hz. The pump beam is first focused onto a small pinhole for selecting the transverse electromagnetic (TEM_{00}) mode and then focused onto the PPLT crystal with a beam size of 80 μm. ASPDC occurs with a threshold of about 69 μJ pump pulse energy, and the measured results can be seen from the output versus pump energy relation in Fig. 4. It shows that for a pump pulse energy of 178 μJ, a maximum output of 35 μJ is achieved, corresponding to a conversion efficiency of 19.7%, or a slope efficiency of 31.5%.

The bandwidth of ASPDC is measured to be $\sim 2\pi \times 502$ GHz by an optical spectrum analyzer. In such a broadband case, two FFPCs centered at the signal and idler wavelengths are used to narrow their bandwidths for the correlation measurement. The FFPC used at the signal path has a $2\pi \times 480$ GHz free spectral range (FSR) and $2\pi \times 2.14$ GHz bandwidth, while the FFPC used at the

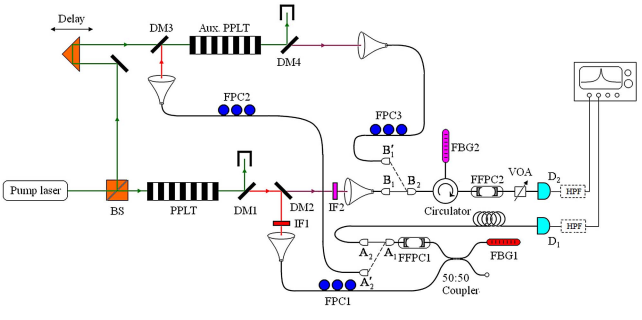

Fig. 3. Schematic of experiment setup. BS, beam splitter; DM, dichromatic mirror; IF, interference filter; FFPC, fiber Fabry–Perot cavity; FPC, fiber polarization controller; FBG, fiber Bragg grating; A_i and B_i, fiber connectors; VOA, variable optical attenuator; HPF, 600 MHz high-pass RF filter (removable).

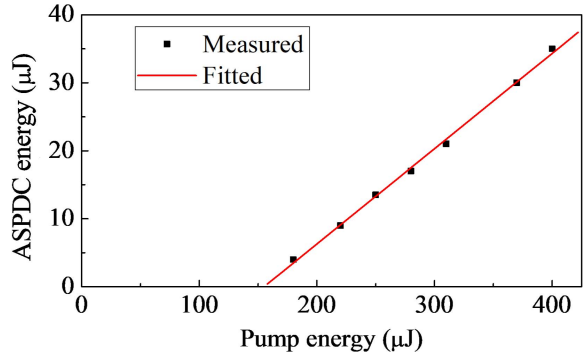

Fig. 4. ASPDC energy as a function of pump pulse energy.

idler path has a $2\pi \times 42$ GHz FSR and $2\pi \times 2.2$ GHz bandwidth, respectively. In order to select only the single-transmission peak of the FFPCs, we used cascaded band-pass filters with bandwidths smaller than the FSR of the corresponding FFPCs. For the signal beam, the band-pass filter consists of a reflective fiber Bragg grating (FBG) (R more than 99.9%) with $2\pi \times 40$ GHz bandwidth and a 50:50 fiber coupler, while for the idler beam, the band-pass filter consists of an FBG with $2\pi \times 12$ GHz bandwidth and a circulator. For frequency-matching and stabilization, all the FFPCs and FBGs are individually temperature-controlled within accuracies of 0.01°C and 0.1°C, respectively. In order to match the center frequency of FFPC2 with those of FFPC1 and pump precisely according to the energy conservation, a difference frequency generation (DFG) process with ω_p and Ω_s is used to generate reference light at Ω_i to stabilize FFPC2. This DFG process happens in an auxiliary identical PPLT crystal with the same poling period when the fiber connectors A_1 and B_2 are connected to A_2' and B_1', respectively (shown as the dash lines in Fig. 3). Then, the output idler beam from the DFG process is sent through FFPC2. By adjusting the temperature of FFPC2, maximum transmission of the idler can be achieved, indicating that FFPC1 and FFPC2 are well matched. Finally, the signal and idler beams are separately detected by GaAs and InGaAs detectors (EOT, ET-4000F and ET-3500F) with less than 30 ps response time, and the system has been well set up for the correlation measurement.

For the correlation measurement, we connect fiber connectors A_1 and B_2 to A_2 and B_1, respectively. A 30 GHz oscilloscope (WaveMaster 830Zi-A, LeCroy) is used to sample and record the photocurrents of the signal and idler beams during the correlation measurement. At pump energy of 164 μJ, the total output energy and peak power of the ASPDC light are 30 μJ and 7.5 kW, respectively. The pulse energies of the signal and idler are measured to be 5.9 nJ and 11 nJ after the spectral filtering, corresponding to the peak powers of 1.48 W and 2.75 W, respectively. Under this condition, we measure the second-order correlation using a pulse train consisting of 100 pulses, as well as the background coming from the same 100 pulses but in random order. The waveforms of the signal and idler beams in the pulse train are recorded, and the second-order correlation function $R^{(2)}$ is calculated by averaging the product of the photocurrents with different relative delay τ, as shown in Fig. 5(a). Both the correlation and background measurements show an envelope with an FWHM of about 4.5 ns, and this is from the contribution of the pulse profile convolution of the signal and idler beams. However, around the zero time-delay point, a sharp peak is observed in the correlation measurement, which is shown in detail by the normalized correlation in Fig. 5(b). The maximum $\gamma^{(2)}$ of 1.43 is achieved, which corresponds to a visibility of 37.9%, and the curve is fitted by an exponential decay function with FWHM of 78 ps. This result agrees well with a theoretical value of 101 ps calculated according to Eq. (5) and Fig. 2. We also study the visibility dependence on pump power and optical loss. The results in Fig. 5(c) show that the visibility almost stays constant in both conditions, which indicates that the correlation between the signal and idler beams is robust to gain change and optical loss. In all of the measurements, the visibility is lower than the theoretical value of about 50%, which may be mainly caused by possible imperfect transverse mode-matching between the signal and idler beams.

More interestingly, the visibility can be further enhanced with electric filtering on the photon current of both detectors. We added a pair of 600 MHz high-pass radio frequency (RF) filters and repeated the correlation measurement. The result is shown in Fig. 5(d). Compared with Fig. 5(a), the background caused by the pulse profile is filtered out, and the visibility is improved up to $97.3\% \pm 2.6\%$.

It should be noted that here we use narrowband optical filters to realize the high-visibility correlation, considering the limited response speed of the photo detectors, which

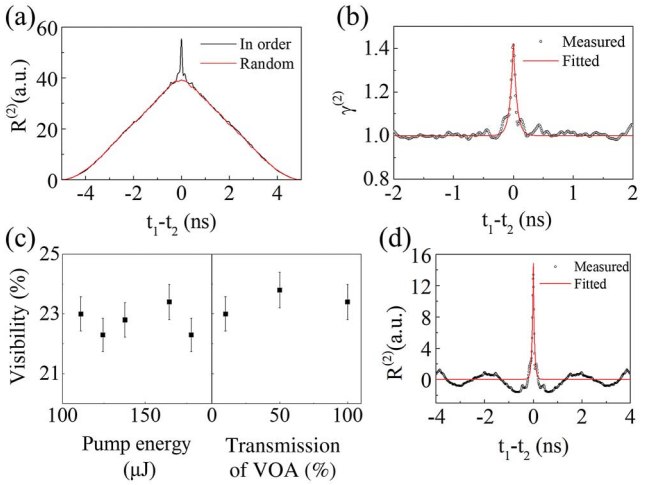

Fig. 5. (a) Correlation of twin beams as a function of relative time delay, where the red curve shows the background given by the pulse profile of the twin beams. (b) Normalized correlation with exponential decay fit. (c) Visibility as a function of pump pulse energy and transmission of variable optical attenuator (VOA), respectively. (d) Correlation measurement with 600 MHz high-pass RF filters in the photon current.

can be selected to be centered at any pair of correlated frequency modes inside the broad ASPDC bandwidth. If the filtering is incorporated with the dense wavelength division multiplexing technique, the channel number can be estimated up to 228, thus showing potential multiplexed applications. However, these filters are not necessary for a narrowband ASPDC source, for example, the backward-wave-type parametric down-converted process[33].

In summary, we reported the observation of a robust second-order correlation between twin parametric beams generated by a high-efficiency ASPDC process and analyzed the physical mechanism behind the correlation as well. Because the spontaneous parametric fluorescence is directly amplified in this process, the twin beams, signal and idler, are built up with a large number of entangled twin-photon pairs. These entangled twin-photon pairs contribute to a temporal correlation that is measurable at macroscopic power levels with similar behavior of SPDC correlation. The visibility of this temporal correlation is directly measured to be 37.9% and can be enhanced to near 100% with electronic filtering on the photon current. In applications, this ASPDC correlation can be used as a high-intensity analog of the SPDC correlation, which is more robust because of much higher efficiency and intensity. These features make it an attractive alternative for many practical applications, such as optical communication and precision measurement. For another application such as the ghost imaging, ASPDC is also a better light source compared to thermal light, because of its inherent correlation feature, which does not require artificial separation of the light to two paths and thus greatly increases the flexibility of a practical imaging system. It also has the special benefits of higher intensity and two-color availability.

This work was supported by the National Key R&D Program of China (Nos. 2019YFA0705000 and 2017YFA0303700) and the National Natural Science Foundation of China (Nos. 51890861, 11690031, 11627810, 11674169, and 11974178). The authors thank Y. H. Shih for valuable discussions and LeCroy Corporation Shanghai Office for the support on the oscilloscope.

References

1. R. Hanbury Brown and R. Q. Twiss, Nature (London) **177**, 27 (1956).
2. R. J. Glauber, Phys. Rev. **130**, 2529 (1963).
3. C. K. Hong, Z. Y. Ou, and L. Mandel, Phys. Rev. Lett. **59**, 2044 (1987).
4. Y. H. Shih and C. O. Alley, Phys. Rev. Lett. **61**, 2921 (1988).
5. J. D. Franson, Phys. Rev. Lett. **62**, 2205 (1989).
6. Z. Y. Ou, X. Y. Zou, L. J. Wang, and L. Mandel, Phys. Rev. Lett. **65**, 321 (1990).
7. P. G. Kwiat, W. A. Vareka, C. K. Hong, H. Nathel, and R. Y. Chiao, Phys. Rev. A **41**, 2910(R) (1990).
8. J. G. Rarity and P. R. Tapster, Phys. Rev. Lett. **64**, 2495 (1990).
9. M. Genovese, Phys. Rep. **413**, 319 (2005).
10. N. Gisin and R. Thew, Nat. Photon. **1**, 165 (2007).
11. P. Kok, W. J. Munro, K. Nemoto, T. C. Ralph, J. P. Dowling, and G. J. Milburn, Rev. Mod. Phys. **79**, 135 (2007).
12. O. S. Magaña-Loaiza and R. W. Boyd, Rep. Prog. Phys. **82**, 124401 (2019).
13. V. Giovannetti, S. Lloyd, and L. Maccone, Science **306**, 1330 (2004).
14. J. L. O'Brien, A. Furusawa, and J. Vučković, Nat. Photon. **3**, 687 (2009).
15. I. Abram, R. K. Raj, J. L. Oudar, and G. Dolique, Phys. Rev. Lett. **57**, 2516 (1986).
16. O. Jedrkiewicz, E. Brambilla, M. Bache, A. Gatti, L. A. Lugiato, and P. Di Trapani, J. Mod. Opt. **53**, 575 (2006).
17. O. A. Ivanova, T. S. Iskhakov, A. N. Penin, and M. V. Chekhova, Quantum Electron. **36**, 951 (2006).
18. F. Sciarrino, C. Vitelli, F. de Martini, R. Glasser, H. Cable, and J. P. Dowling, Phys. Rev. A **77**, 012324 (2008).
19. T. Iskhakov, M. V. Chekhova, and G. Leuchs, Phys. Rev. Lett. **102**, 183602 (2009).
20. F. Boitier, A. Godard, N. Dubreuil, P. Delaye, C. Fabre, and E. Rosencher, Nat. Commun. **2**, 425 (2011).
21. A. Allevi, S. Olivares, and M. Bondani, Phys. Rev. A **85**, 063835 (2012).
22. T. S. Iskhakov, K. Y. Spasibko, M. V. Chekhova, and G. Leuchs, New J. Phys. **15**, 093036 (2013).
23. Q. Zhang, X. Deng, C. Tian, and X. Su, Opt. Lett. **42**, 895 (2017).
24. X. Su, A. Tan, X. Jia, Q. Pan, C. Xie, and K. Peng, Opt. Lett. **31**, 1133 (2006).
25. J. Mertz, T. Debuisschert, A. Heidmann, C. Fabre, and E. Giacobino, Opt. Lett. **16**, 1234 (1991).
26. A. S. Villar, L. S. Cruz, K. N. Cassemiro, M. Martinelli, and P. Nussenzveig, Phys. Rev. Lett. **95**, 243603 (2005).
27. X. Jia, Z. Yan, Z. Duan, X. Su, H. Wang, C. Xie, and K. Peng, Phys. Rev. Lett. **109**, 253604 (2012).
28. T. P. Lee, C. A. Bums, and B. I. Miller, IEEE J. Quantum Electron. **19**, 820 (1973).
29. J. Boeck and M. C. Amadn, Frequenz **33**, 278 (1979).
30. M. Blazek, S. Hartmann, A. Molitor, and W. Elsaesser, Opt. Lett. **36**, 3455 (2011).
31. R. W. Boyd, *Nonlinear Optics*, 2nd ed. (Academic, 2003).
32. K. Wodkiewicz and J. H. Eberly, J. Opt. Soc. Am. B **2**, 458 (1985).
33. C. Canalias and V. Pasiskevicius, Nat. Photon. **1**, 459 (2007).